Progress in Nuclear Energy, 1982, Vol. 9, pp. 75-82
Printed in Great Britain. All rights reserved

0079-6530/82/030075-08$4.00/0

APPLICATION OF NEUTRON NOISE ANALYSIS TO A SWIMMING POOL RESEARCH REACTOR

K. BEHRINGER, V. H. LESCANO, F. MEIER, J. PHILDIUS and H. WINKLER

Swiss Federal Institute for Reactor Research (EIR) CH-5303 Würenlingen, Switzerland

ABSTRACT

This work is part of a programme of establishing practical applications of neutron noise techniques to a swimming pool research reactor and deals with two different items : (1) The identification of local boiling caused e.g. by a partial blockage of the coolant flow in a fuel element. Local boiling can easily lead to a burn-out situation. The onset of boiling can be detected by neutron noise analysis and a boiling detection system is presently under development. (2) The measurement of the time evolution of the reactivity induced by xenon after reactor shut-down by an on-line reactivity meter based on neutron noise analysis. From the data, the prompt neutron decay constant at delayed critical, the equilibrium xenon reactivity worth, and an estimate of the average steady-state power flux in the core before reactor shut-down were obtained.

KEYWORDS

Reactor noise analysis, neutron noise, boiling detection, xenon poisoning, swimming pool type reactors.

INTRODUCTION

The noise investigations briefly reported in this paper are part of a programme of establishing practical applications of neutron noise techniques to the swimming pool type reactor SAPHIR at EIR, Switzerland. They concern two different items :

- Boiling detection

The first item deals with the detection of boiling and is a power neutron noise application. SAPHIR is normally operated at a power level of 5 MW with forced coolant water convection. The appearance of local boiling is a safety-related operational problem because it can easily lead to burn-out. Therefore, the development and installation of an appropriate surveillance system capable of detecting the onset of boiling can reduce the danger of burn-out. Neutron noise investigations under controlled boiling conditions show that boiling induces reactivity fluctuations which significantly increase the noise signal amplitudes in the frequency range below 5 Hz. A prototype boiling detection system is presently under development. It is based on simple amplitude thresholding and uses existing control instrumentation.

- Xenon poisoning

The second item refers to the determination of reactor operational parameters by an on-line reactivity meter under zero-power conditions, in this case, applied to the measurement of the time evolution of xenon poisoning after a reactor shut-down from a preceeding stationary power operation. From the data, the prompt neutron decay constant at delayed critical, the equilibrium xenon reactivity worth, and an estimate of the core-average steady-state thermal flux at power (thermal power flux) were obtained by means of a simple space-dependent theory of the xenon poisoning.

BOILING DETECTION

The coolant flow at SAPHIR is a forced down-stream of the pool water through the water gaps between the fuel plates. There are 3 circulation pumps and the total coolant flow rate is about 130 ℓ/s. The onset of local boiling causes changes in the coolant flow distribution. This can lead to flow instabilities and, under advanced boiling conditions, to superheated fuel plates which may result in a burn-out situation. Several investigations (Wittle and Forgan, 1967; Fries et al., 1972; Winkler, 1976) which are partially based on mock-up experiments, allow a reliable prediction of the critical power densities. These data are sufficient for the design of safe coolant flow conditions.

Due to a risk study performed for SAPHIR, the most probable event that can initiate boiling is the partial blockage of one or two cooling channels of a fuel element by foreign substances, e.g. by plastics which can fall in the pool. A partial melting of one or more fuel plates does not endanger the environment. Such an incident, however, should be avoided by the installation of a surveillance system which detects the onset of boiling but does not give false alarms under normal operation conditions. A detection time of about half a minute after the onset of boiling is to be regarded as sufficient. There is no requirement of localizing any boiling fuel element channel.

The core of the reactor SAPHIR consists of highly enriched uranium fuel elements and is small compared to the usual size of a power plant reactor. Local void fluctuations are therefore expected to induce additional reactivity fluctuations which are stronger than the reactivity fluctuations existing during normal reactor operation (Winkler and Zeis, 1977).

The first experiment was performed under reduced coolant flow rate with one pump in operation (47 ℓ/s). The reactor power was increased in small steps until at a power level of 2.97 MW the initiation of boiling in 3 water gaps was observed by a telescope. The onset of boiling can be recognized by the visible flow streamlines produced by the water turbulence above a boiling channel which induce fluctuating shadow effects on the Cerenkov light. It was visually observed that boiling does not start immediately after the minimum required power level has been reached, but with a delay of several minutes. This is due to rearrangement of the coolant flow distribution. Boiling begins in the water gaps between the fuel plates which have the highest surface temperature and spreads out slowly in time with increasing intensity to other channels.

The onset of boiling is also manifested in the neutron noise. For the neutron noise measurements, two boron ionization chambers located in the reflector near the core boundaries were used. Fig. 1 shows two signal patterns, the one measured after boiling has just started, the other measured under no boiling condition after the coolant flow has been increased by switching on the other two circulation pumps. Boiling is characterized by the appearance of marked "boiling pulses" which were found to be coincident between both measuring channels.

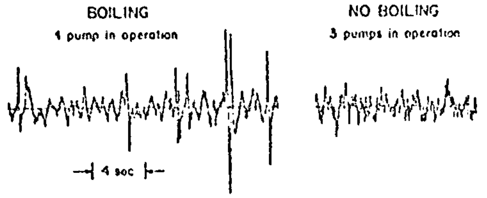

Fig. 1 . Neutron noise signal, first experiment, reactor power 2.97 MW. (band-pass filtered 1-40 Hz)

The appearance of these boiling pulses was not observed during a second experiment which was performed under different thermal-hydraulic conditions. Here, the reactor power was kept constant at a level of 5.2 MW. The initial coolant flow rate of 126.5 ℓ/s with 3 pumps in operation was stepwise reduced. First concrete indication of boiling appeared at a coolant flow rate of 96.6 ℓ/s. Fig. 2 shows the signal patterns with and without boiling. In contrast to Fig. 1, there is no obvious visible structure in the presence of boiling. Boiling manifests itself by a general increase of the noise amplitudes at low frequencies.

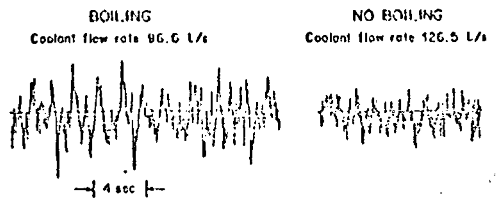

Fig. 2 . Neutron noise signal, second experiment, reactor power 5.2 MW. (band-pass filtered 1-40 Hz)

Figs. 3 and 4 show neutron APSDs measured in the first and the second experiment respectively under reactor conditions with and without local boiling of the coolant. The measuring time was about 4 minutes in each case. CPSD-measurements confirmed that all useful information in the noise signals is contained in the frequency range below approximately 12 Hz.

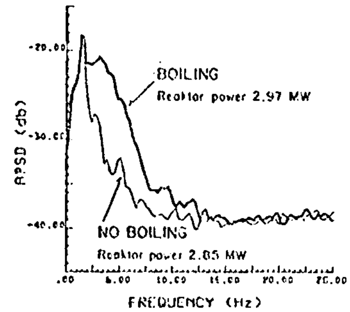

Fig. 3 . Neutron APSDs, first experiment, 1 pump in operation. (1 Hz high-pass filtering)

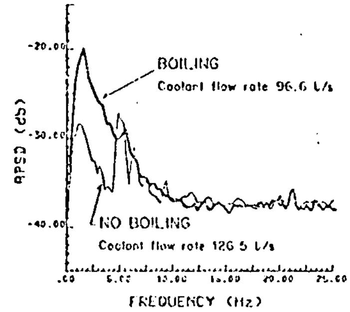

Fig. 4 . Neutron APSDs, second experiment, reactor power 5.2 MW. (1 Hz high-pass filtering)

The features observed in the measurements can at least qualitatively be understood when one considers the theoretical APSD of the current signal fluctuations of a neutron detector. If one neglects the fluctuations due to the neutron branching process, the APSD is given in the point kinetics model by (Albrecht, 1972)

$$\mathrm{APSD}(\omega) = WF\overline{q^2} + W^2F^2\bar{q}^2\,|H(\omega)|^2\,|\rho(\omega)|^2 \qquad (1)$$

where W is the detector efficiency (counts/fission), F is the fission rate in the system, q is the charge released per neutron detected, $H(\omega)$ is the overall reactivity transfer function including feedback, and $|\rho(\omega)|^2$ is the power spectral density of the reactivity fluctuations which, in the presence of boiling, can be decomposed into a normal and an anomalous part :

$$|\rho(\omega)|^2 = |\rho_n(\omega)|^2 + |\rho_a(\omega)|^2 \qquad (2)$$

The first term in eq.(1) is due to uncorrelated detection noise which is frequency independent and appears in Figs. 3 and 4 as the dominant contribution above 12 Hz. The second term in eq. (1) is the power noise term and is dominant in the frequency range below 12 Hz. Fig. 3 shows that in this low frequency range additional boiling results in an almost equal amplitude elevation in the spectra. Such behaviour is to be expected if the anomalous reactivity fluctuations in eq.(2) are approximately white noise. However, under the different thermal-hydraulic conditions of the second experiment, Fig. 4 shows that the anomalous noise due to boiling seems to be confined to frequencies not exceeding approximately 8 Hz. Both experiments imply that the frequency range up to about 5 Hz is the most important for the boiling detection. The significant peak at 5 Hz and others appearing in the spectra can be attributed to structure vibrations (and the servo-control) because they are also observable (although not always exactly at the same frequency positions and with the same intensities) in the zero-power neutron noise spectra under forced coolant convection conditions.

In the control instrumentation of SAPHIR, there are two linear flux channels with γ-compensated boron chambers and three linear safety channels with uncompensated boron chambers. The safety channels were found to be less suitable for connecting a boiling detector because these chambers have about 3 times lower efficiency than the chambers in the flux channels. Fig. 5 shows

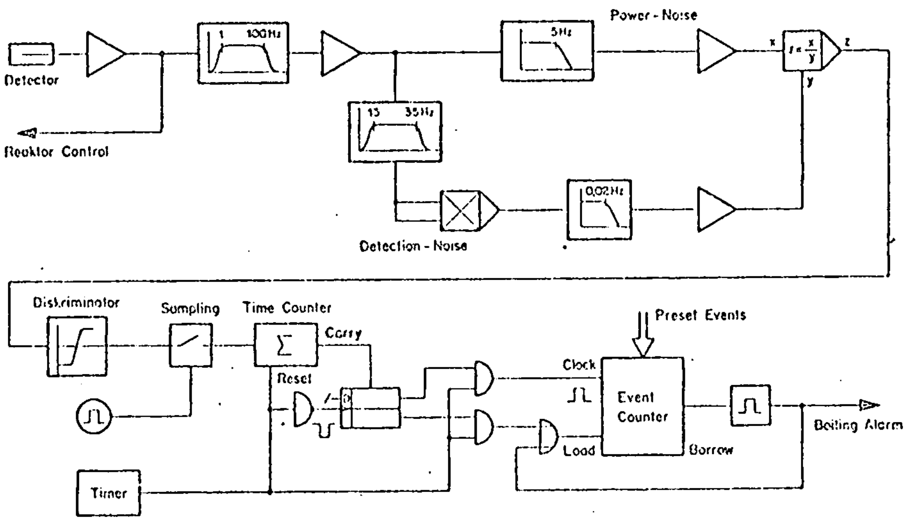

Fig. 5 . Block diagram of the boiling detector

the block diagram of the developed prototype boiling detector. There are two units, each connected to one of the two independent amplifier outputs of the flux channels. The equipment uses simple amplitude threshold techniques. When the amplitude of the 1 - 5 Hz band-pass filtered noise signals exceeds a given level (presently set at 150 % of the normal peak noise amplitude), a Schmitt-circuit is triggered. Its output signal is time-integrated by sampling techniques. The integral value is stored in a "time" counter which is reset every 5 seconds. If within a reset period the number of pulses stored in the time-counter exceeds a preset value corresponding to a total time sum of 10 % of the reset period, a 1 is added to an "event" counter. If in the immediately following reset period there are fewer counts in the time-counter than that given by its preset level, the event-counter will be reset, otherwise it will continue to count until a preset value of "events" is reached which initiates an alarm of duration of several seconds. The cycle is then repeated. The equipment contains a limited automatic gain control which, according to eq.(1), uses the variance of the detection noise component in the frequency range 15 - 35 Hz in order to be independent of the selected power level within the range of interest.

The concept of the equipment implies discrimination against sporadically appearing large amplitudes in the normal power noise due to statistics, and short term perturbations produced e.g. by switching operations in the reactor control and fine control rod movements by the servo. The preliminary experience shows that false alarms can occur (a) during reactor start-up until an almost stable power operation has been reached (and obviously during a shut-down), (b) by an external perturbation of the neutron field, e.g. when an operator inserts or removes an irradiation probe at the core surface, or by a vibrating irradiation probe which is not well fixed in the holder. As long as such "false" alarms can be easily identified, it is believed that they are useful for a periodic check of the equipment performance.

Finally, it should be noted that acoustic emission noise produced by the bubble collapse can also be utilized for detecting the onset of boiling. On the other hand, this method was found to be very sensitive to background noise and needs further investigation. The neutron noise technique, however, is a simple method and has the advantage that the existing detectors of the reactor control instrumentation can be used.

XENON POISONING

The aim of the measurement of xenon poisoning is to demonstrate the practical application of zero-power neutron noise analysis for extracting reactor operational parameters the values of which can be used for code verification. The measurement was performed with an on-line reactivity meter which is based on the "Zero-Crossing Correlation Method" (Behringer et al., 1975) and uses polarity cross-correlation techniques with a two-detector measuring device (for a block diagram of the equipment and a study of the display variance see Behringer and Peier, 1979). The meter covers a reactivity range down to about -5 \$. The amplifiers consist of a recently improved system containing automatic DC-offset, input sensitivity control, and gain control to follow slowly varying reactor conditions by self-adjustment.

The detectors were highly efficient He-3 filled ionization chambers located in the reflector near the core edges. Previous experimental and theoretical investigations (Lescano and Behringer, 1981) have shown that under such measuring conditions, space-energy effects in the required frequency range (15 to 200 Hz) of the neutron noise are negligibly small. The use of the point kinetics model was found to be a good approximation in the analysis.

Two measurements of the time evolution of the xenon poisoning after reactor shut-down were performed at different core configurations and with different ex-core detector locations. Here, the discussion is limited to part of the second measurement only. A complete description of the experiments and the results will be given in a later publication.

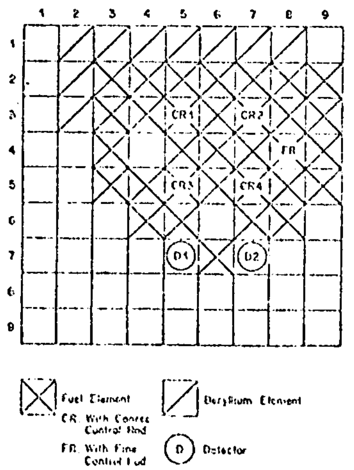

Fig. 6 . SAPHIR core configuration 392 B .

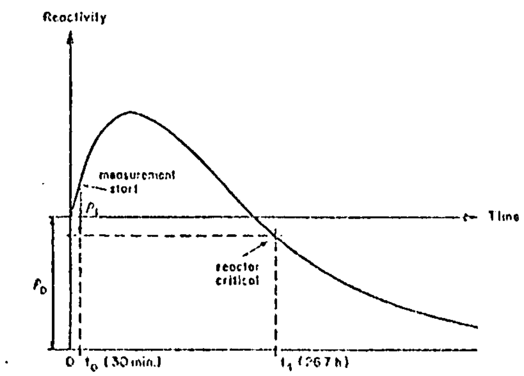

Fig. 7 . Evolution of the measurement and reactivity balance.

The core configuration is shown in Fig. 6. The reactor was operated at a steady-state power level of about 5 KW during several weeks before shut-down. The position of the 4 coarse control rods was near the upper limit at the end of the power operation period. The evolution of the measurement is schematically represented in Fig. 7. After reactor shut-down at t=0, the detectors were inserted at the positions shown in Fig. 6, and all control rods were withdrawn from the core. Due to the build-up of the xenon poisoning and the reactivity worth of the detectors, the reactor could not be made critical again. At t_0, i.e. 30 minutes after shut-down, the reactivity measurement started and continued during the time of the xenon peak evolution without any change in the reactor conditions until the time when the reactor reached the level of 5 KW by itself, about 27 hours after shut-down. The reactor was then maintained at this power level for a short time by reactivity compensation using the fine control rod. Since during this time the xenon poisoning decreases linearly with time, an extrapolation backward in time from two reactivity values of the fine control rod permitted the exact determination of the time instant t_1 when the reactor became critical by itself. For the subcritical measurements no extraneous neutron source was used. The photo-neutrons from (γ,n) reactions form a sufficiently strong natural source of fast neutrons.

Using for convenience positive subcritical reactivity values in units of dollars, the reactivity balance in the measuring time interval $t_0 \leq t \leq t_1$ (see Fig. 7) is given by

$$\rho(t) = \rho_i + \rho_{Xe}(t) - \rho_{Xe}(t_0) \tag{3}$$

where ρ_i is the initial reactivity at t_0. The reactivity $\rho_{Xe}(t)$ introduced by the xenon can be written as a sum of two terms.

$$\rho_{Xe}(t) = \rho_0 F(t) + \rho_1 G(t) \tag{4}$$

where $F(t) = e^{-\lambda_{Xe} t}$, $G(t) = e^{-\lambda_{Xe} t} - e^{-\lambda_I t}$, and λ_{Xe}, λ_I are the decay constants of Xe-135 and I-135 respectively. The first term on the rhs. of eq.(4) is due to the decay of the Xe-135 nuclei present at t=0, and the second term arises from the xenon production via the decay of the I-135 nuclei.

The reactivity meter continuously indicates the zero-crossing point τ_0 of the cross-correlation function. From a measurement of τ_0, and using the point kinetics approach one obtains the prompt neutron decay constant α by solving a transcendental equation numerically. Writing

$$\alpha(t) = \alpha_c(1 + \rho(t)) \tag{5}$$

where α_c is the prompt neutron decay constant at delayed critical, one obtains the equation :

$$\alpha(t) = \underbrace{\alpha_c(1+\rho_i)}_{x_1}\{1 + \underbrace{\frac{\rho_0}{1+\rho_i}}_{x_2}(F(t)-F(t_0)) + \underbrace{\frac{\rho_1}{1+\rho_i}}_{x_3}(G(t)-G(t_0))\} \tag{6}$$

The rhs. of eq.(6) contains 3 unknown quantities, x_1, x_2 and x_3 which can be determined by a least squares fit to the measured $\alpha(t)$ curve. After a determination of these quantities, ρ_i can be eliminated by applying the criticality condition at t_1 to eq.(3), i.e. $\rho(t_1) = 0$. One then obtains the values of α_c, ρ_0 and ρ_1.

Fig. 8 shows the measured time evolution of the xenon reactivity and the theoretical curve obtained from eq.(4) with the fitted parameters ρ_0 and ρ_1. The relatively large statistical fluctuations in the measurement result from the fact that a relatively small value for the averaging time (order of magnitude of several minutes) was used in the correlator.

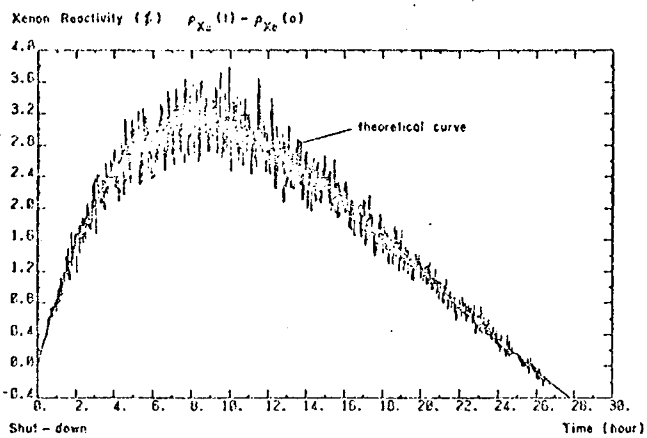

Fig. 8 . Time evolution of the xenon-peak.

For α_C , a value of 114 ± 1 sec^{-1} was obtained. This value is in excellent agreement with a direct determination of this quantity where a value $\alpha_C = 115 \pm 4$ sec^{-1} resulted from several measurements at criticality. The reactivity effects induced by the xenon depend on the reactor power and the termal flux distribution. The values obtained for ρ_0 and ρ_1 (see Table 1) were used for estimating the core-average thermal power flux. From a CODIFF-calculation, a value of the core-average thermal power flux (within $\pm$ 5 % due to the accuracy of the reactor power calibration) as well as the radial flux distribution for the actual core configuration under burn-up conditions were available. CODIFF is a two-dimensional multi-group diffusion code for static flux calculations, and is a further development of DIFFUS. Both codes have been developed by Paratte (1973).

Assuming that the thermal flux distribution in the subcritical reactor has almost the same shape as when the reactor is at power and using first order perturbation theory, the average thermal power flux $\bar{\Phi}$ can be obtained from the ratio ρ_1/ρ_0 which is given by

$$\frac{\rho_1}{\rho_0} = \frac{\gamma_I}{\gamma_I + \gamma_{Xe}} \frac{\lambda_{Xe}}{\lambda_I - \lambda_{Xe}} (1+A)S \qquad (7)$$

where γ_{Xe} and γ_I are the fractional yields of Xe-135 and I-135 respectively. The quantity A is given by

$$A = \sigma_{Xe}\bar{\Phi}/\lambda_{Xe} \qquad (8)$$

where σ_{Xe} is the microscopic cross-section for thermal neutron capture in Xe-135. S is a shape factor given by

$$S = \frac{1}{1+A} \frac{\int dV\, \Sigma_f \phi^3}{\int dV \frac{\Sigma_f \phi^3}{1+AC\phi}} \qquad (9)$$

where Σ_f is the macroscopic fission cross-section. ϕ is the normalized thermal flux distribution (Φ_{max} = 1), and C = $\Phi_{max}/\bar{\Phi}$. C describes the non-uniformity of the flux distribution in the core. In an infinite homogeneous medium, S becomes equal to 1 . Wenzel (1961) investigated the integrals in eq.(9) for homogeneous cores. He found that for extrapolated lengths up to 20 % of the linear core dimensions, the shape factor S can be expressed as a linear function of the quantity C and is practically independent of the reactor geometry.

Unfortunately, measured flux distributions were not available. Therefore, several cases of flux distributions were considered for estimating $\bar{\Phi}$ and the results are shown in Table 1 .

TABLE 1 Estimated average thermal flux values

EXPERIMENTAL DATA: ρ_0 = 3.76 ± 0.03 \$
ρ_1 = 4.29 ± 0.4 \$

REACTOR POWER: 5.3 ± 5 % MW
$\bar{\Phi}$ = (2.72 ± 0.14) × 10^{13} N/CM^2 SEC (CODIFF)

CASE	ASSUMED FLUX DISTRIBUTION	S	$\bar{\Phi}$ (N/CM^2 SEC) ×10^{13}
1	$\varphi(\vec{x})$ = CONSTANT	1.	3.32
2	$\varphi(\vec{x})$ = COS (BX) COS (BY) COS (BZ)	1.40	2.29
3	φ (X,Y) : CODIFF φ (Z) = CONSTANT	1.18	2.67
4	φ (X,Y) : CODIFF φ (Z) = COS (BZ)	1.30	2.35

When one assumes a uniform flux distribution throughout the core, an upper limit value for $\bar{\Phi}$ is obtained. A lower limit value is expected when one regards a homogeneous cubic core with cosine-flux distribution in all directions. In the cases 3 and 4, the estimates use the radial flux distribution calculated by CODIFF. Case 3 assumes a uniform axial flux distribution whereas case 4 assumes a cosine-distribution. The best agreement between the calculated and "semi-experimental" average flux values is for case 3. This may be due to the fact that in this core configuration the central region of the core contained fuel elements with a very high burn-up (40-60 %). This flattens the flux distribution in the core.

ACKNOWLEDGEMENTS

We are indebted to Mr.R.Crowe for his assistance in the first boiling noise investigations. He and also Dr.D.Lübbesmeyer helped in the xenon poisoning measurements. Mr.B.Leoni had to solve several technical problems in the built-up and installation of the measuring equipments. Mr.P. Koehler performed the CODIFF-calculations. Thanks are due to the SAPHIR operators for their support during the investigations.

REFERENCES

Albrecht R.W. (1972). Nucl.Technology 14, 208
Behringer K., Phildius J., and Seifritz W. (1975). Ann.Nucl.Energy 2, 399
Behringer K., and Peier W. (1979). Nucl.Instr.Methods 161, 97
Fries S., Hofmann K., and Petersen G. (1972). GKSS 72/E/30 (Gesellschaft für Kernenergieverwertung in Schiffbau und Schiffahrt, Geesthacht)
Lescano V.H., and Behringer K. (1981). Paper submitted to Ann.Nucl.Energy.
Paratte J.M. (1973). EIR-report 232
Wenzel P. (1961). Kernenergie 4, 775 and 926
Winkler H. (1976). Internal EIR-report TM-SR-106
Winkler H., and Zeis J. (1977). Internal EIR-report TM-SR-108
Wittle R.H., and Forgan R. (1967). AERE-M-1939 Part 1+2